Cross-linking of Orai1 channels by STIM proteins

Yandong Zhou[a,1,2], Robert M. Nwokonko[a,1], Xiangyu Cai[a], Natalia A. Loktionova[a], Raz Abdulqadir[a], Ping Xin[a], Barbara A. Niemeyer[b], Youjun Wang[c], Mohamed Trebak (محمد طريبق)[a], and Donald L. Gill[a,2]

[a]Department of Cellular and Molecular Physiology, Pennsylvania State University College of Medicine, Hershey, PA 17033; [b]Department of Molecular Biophysics, Center for Integrative Physiology and Molecular Medicine, Saarland University, Homburg 66421, Germany; and [c]Beijing Key Laboratory of Gene Resources and Molecular Development, College of Life Sciences, Beijing Normal University, 100875 Beijing, People's Republic of China

The transmembrane docking of endoplasmic reticulum (ER) Ca^{2+}-sensing STIM proteins with plasma membrane (PM) Orai Ca^{2+} channels is a critical but poorly understood step in Ca^{2+} signal generation. STIM1 protein dimers unfold to expose a discrete STIM–Orai activating region (SOAR1) that tethers and activates Orai1 channels within discrete ER–PM junctions. We reveal that each monomer within the SOAR dimer interacts independently with single Orai1 subunits to mediate cross-linking between Orai1 channels. Superresolution imaging and mobility measured by fluorescence recovery after photobleaching reveal that SOAR dimer cross-linking leads to substantial Orai1 channel clustering, resulting in increased efficacy and cooperativity of Orai1 channel function. A concatenated SOAR1 heterodimer containing one monomer point mutated at its critical Orai1 binding residue (F394H), although fully activating Orai channels, is completely defective in cross-linking Orai1 channels. Importantly, the naturally occurring STIM2 variant, STIM2.1, has an eight-amino acid insert in its SOAR unit that renders it functionally identical to the F394H mutant in SOAR1. Contrary to earlier predictions, the SOAR1–SOAR2.1 heterodimer fully activates Orai1 channels but prevents cross-linking and clustering of channels. Interestingly, combined expression of full-length STIM1 with STIM2.1 in a 5:1 ratio causes suppression of sustained agonist-induced Ca^{2+} oscillations and protects cells from Ca^{2+} overload, resulting from high agonist-induced Ca^{2+} release. Thus, STIM2.1 exerts a powerful regulatory effect on signal generation likely through preventing Orai1 channel cross-linking. Overall, STIM-mediated cross-linking of Orai1 channels is a hitherto unrecognized functional paradigm that likely provides an organizational microenvironment within ER–PM junctions with important functional impact on Ca^{2+} signal generation.

calcium signals | Orai channels | STIM1 protein | STIM2.1 protein | calcium oscillation

The STIM proteins, STIM1 and STIM2, function as sensors of Ca^{2+} stored within the endoplasmic reticulum (ER) (1–7). In response to depletion of Ca^{2+} stored in the ER, the cytoplasmic STIM1 C-terminal domain unfolds and attaches to the PM, causing STIM1 to be trapped within ER–PM junctions (1–7). The unfolding process exposes a small, highly conserved STIM–Orai activating region (SOAR1) within STIM1 which is able to tether and activate the Orai family of PM Ca^{2+} entry channels within the ER–PM junctions (8–10). The "store-operated" Ca^{2+} entry (SOCE) through Orai1 channels is crucial in sustaining Ca^{2+} oscillations and mediating local Ca^{2+} signals that control gene expression (1, 3–5, 11, 12). Although the interaction between STIM and Orai proteins is clearly observable, much is still not understood about their association and organization within junctions and how these interactions mediate the generation of Ca^{2+} signals (3–7, 13).

The STIM1 protein exists as a dimer within the ER membrane (10, 14) and appears to remain dimeric during store depletion-induced activation and interaction with Orai1 (1, 3). The tightly folded SOAR1 unit within STIM1 is an important locus for its dimerization (10, 14–16). The SOAR1 dimer likely remains intact during the store depletion-induced unfolding of STIM1 and the subsequent association of SOAR1 with the Orai1 channel

(15, 17, 18). It had been suggested that Orai1 channel activation occurs following a "bimolecular" interaction of the SOAR1 dimer in STIM1 with a pair of adjacent Orai1 subunits within the hexameric Orai1 channel (19–22). We recently revealed that the exposed F394 residue in SOAR1 plays a pivotal role in both binding to and gating of the Orai1 channel (23). F394 mutated to histidine, completely blocks the Orai1 interaction yet does not affect full-length STIM1 activation or entry into ER–PM junctions. Unexpectedly, we determined that mutation of just one of the two F394 residues in the concatenated SOAR1 dimer still resulted in full Orai1 channel activation (17). This indicates that each monomer in the SOAR dimer can independently undergo a "unimolecular" interaction with a single Orai1 subunit, and this interaction is sufficient to gate the Orai1 channel (17, 24). This model is quite different from the bimolecular interaction with Orai1 subunits envisaged earlier and also explains why Orai1 channel activation can occur with a STIM1: Orai1 ratio of 2:1 (25, 26). Since unimolecular coupling requires only one active site on the SOAR1 dimer to activate the Orai1 channel, we suggested that the other site would be available to undergo interaction with a subunit on another channel (17).

Here we reveal strong evidence that the SOAR1 dimer from STIM1 can indeed mediate cross-linking between Orai1 channels. We provide high-resolution imaging, biophysical, and functional evidence for SOAR-induced cross-linking of Orai1 channels. We observe that the single F394H mutation in the Orai1 binding site completely prevents this cross-linking. We also investigate an

Significance

The work presents a unique understanding of the organization and function of two ubiquitously expressed proteins, central in generating calcium signals in all cell types. These are the intracellular calcium sensing "STIM" proteins, and the highly selective cell surface "Orai" calcium channels. We reveal that STIM proteins can cross-link Orai channels, resulting in a reorganized microenvironment within the membrane junctions in which they function, with important consequences in the generation of oscillatory calcium signals. Interestingly, we show a variant STIM protein widely expressed in cells functions to prevent the STIM–Orai cross-linking and clustering of channels. This provides important modulation of calcium signal generation and can serve to protect cells from overstimulation of the calcium signaling machinery.

interesting and widely expressed splice variant of STIM2 (STIM2.1 or STIM2β) (27, 28) which is shown to be defective in Orai1 binding by virtue of an eight-amino acid insert within the SOAR sequence, close to the Orai1-interacting site. Using concatenated SOAR constructs, we reveal that the naturally occurring STIM2.1 variant is functionally equivalent to the F394H STIM1 mutant. In contrast to predictions that STIM2.1 dominantly suppresses STIM1 (28), we observe that SOAR heterodimers containing SOAR units from both STIM1 and STIM2.1 are able to fully activate Orai1 channels. However, such SOAR heterodimers are defective in cross-linking Orai1 channels, indicating that STIM2.1 functions to prevent STIM1-mediated Orai1 cross-linking. Interestingly, the combined expression of full-length STIM1 with STIM2.1 results in suppression of agonist-induced Ca^{2+} oscillations, likely as a result of diminished Orai1 channel cross-linking. We suggest that although activated STIM proteins localize within discrete ER–PM junctional domains, the STIM-mediated cross-linking of Orai channels within these domains provides an organizational microenvironment that has important functional impact on the generation of Ca^{2+} signals.

Results and Discussion

SOAR Dimers Are Able to Cross-Link and Cluster Orai1 Channels. Orai channels exist and function as hexamers (29–32) that freely diffuse in the PM before undergoing a reversible interaction with STIM1 in ER–PM junctions (33). From our recent studies revealing a unimolecular interaction of SOAR dimers with Orai1 channel subunits, we predicted that wild-type SOAR1 dimers (YFP-S-S in Fig. 1A) might cross-link Orai1 channels by interacting with channel subunits in separate Orai1 hexamers (17). Although SOAR heterodimers containing a single F394H mutation could still undergo unimolecular binding and activation of Orai1 channels (17), we expected that they would not cross-link between channels. However, we observed no difference in the distribution of wild-type YFP–SOAR1 homodimers compared with YFP–SOAR1 heterodimers with a single F394H mutation (YFP-S_H-S or YFP-S-S_H in Fig. 1A)
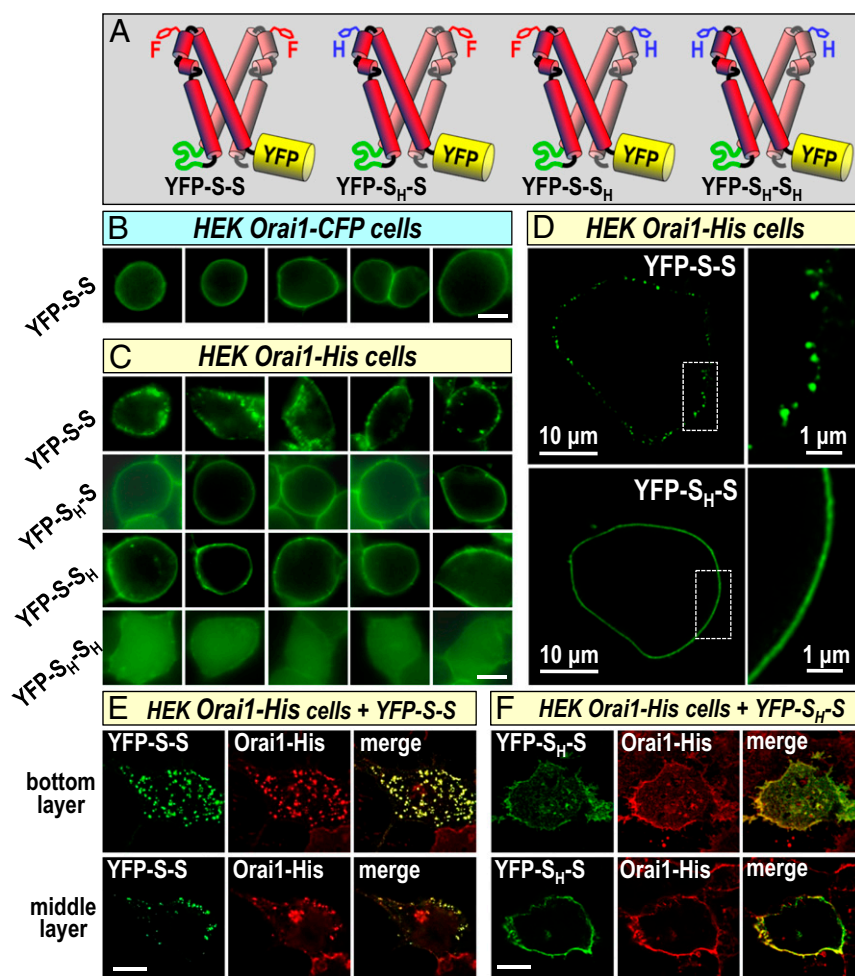

Fig. 1. Cross-linking of SOAR dimers and Orai1 channels to form clusters. (A) YFP-labeled concatenated SOAR dimers. From the *Top*: wild-type SOAR1 homodimer (YFP-S-S), SOAR1^{F394H}–SOAR1 heterodimer (YFP-S_H-S); YFP–SOAR1–SOAR1^{F394H} heterodimer (YFP-S-S_H); YFP–SOAR^{F394H}–SOAR^{F394H} mutant homodimer (YFP-S_H-S_H). (B) Expressed in stable HEK Orai1–CFP cells, the YFP-S-S SOAR homodimer is localized to the PM but shows no clustering. (C) YFP-S-S expressed in stable HEK Orai1–His cells shows distinct PM-localized clusters (*Top* row), whereas the YFP-S_H-S (*Middle* row) and YFP-S-S_H (*Bottom* row) heterodimers do not cluster. The mutant homodimer YFP-S_H-S_H remains cytosolic and does not bind to Orai1. (D) Stimulated emission depletion (STED) images of YFP-S-S SOAR dimers (*Top*) expressed in HEK Orai1–His cells revealing clear, discrete PM-localized clusters up to 200 nm, whereas the YFP-S_H-S heterodimer (*Bottom*) identically expressed has a PM localized but entirely smooth appearance. (E and F) Confocal images of HEK Orai1–His cells expressing either YFP-S-S (E) or YFP-S_H-S (F); immunofluorescence staining used an anti-GFP antibody to target YFP–SOAR dimers (green), and an anti-hOrai1 antibody targeting Orai1–His (red). Images are from the bottom of cells (*Top* images) or from the middle of cells (*Bottom* images). Merged images reveal clear PM localization of YFP-S-S and Orai1–His in almost completely overlapping clusters (E), whereas localization of YFP-S_H-S and Orai1–His was PM localized but not clustered (F). (Scale bars, 10 μm unless otherwise marked.) Images are representative of 3–10 separate experiments.

when expressed with Orai1–CFP (17). We recently reported that STIM1 binding to the cytosolic Orai1 C-terminal domain is sufficient to mediate opening of the channel (24). However, addition of large fluorescent tags to the C terminus of Orai1 does not alter the function of Orai1 or its activation by STIM1 (31, 34, 35). Although the Orai1 C-terminal CFP tag does not prevent STIM1 binding per se, we considered that this bulky addition to each Orai1 subunit might sterically prevent the STIM1-mediated cross-linking of Orai1 channels (*SI Appendix*, Fig. S1A). We therefore compared distribution of SOAR dimers in HEK cells stably expressing Orai1 channels C-terminally tagged with the small 5-amino acid His tag as opposed to the large 275-amino acid CFP tag. As shown in Fig. 1B, the YFP-S-S homodimer expressed in HEK Orai1–CFP cells, was distributed entirely evenly across the PM. In contrast, YFP-S-S expressed in HEK Orai–His cells was profoundly punctal in appearance, with an obvious clustered distribution (Fig. 1C, *Top*). However, YFP-S_H-S or YFP-S-S_H expressed in the same HEK Orai1–His cells, had a smooth, even distribution across the PM (Fig. 1C, second and third rows). As expected, the YFP-S_H-S_H F394H homodimer was not associated with the membrane (Fig. 1C, *Bottom*), thus the interaction of SOAR dimer constructs with the PM was entirely dependent on Orai1 channels. Models depicting YFP-S-S–mediated Orai1–His cross-linking and the lack of cross-linking by YFP-S_H-S, are shown in *SI Appendix*, Fig. S1 *B* and *C*, respectively.

Although these live-cell epifluorescence images revealed that the His-tagged Orai1 construct permitted a profoundly distinct punctal distribution of the YFP-S-S homodimer, we sought to obtain superresolution images using stimulated emission depletion (STED) microscopy. As shown in Fig. 1D, *Top*, the appearance of the YFP-S-S homodimer on the PM surface of HEK Orai1–His cells was entirely within discrete, clearly defined clusters varying in size up to ∼100–200 nm. In contrast, the same high-resolution STED imaging in cells expressing the YFP-S_H-S heterodimer revealed a clean, continuous distribution (Fig. 1D, *Bottom*). The images provide strong evidence that the SOAR1 dimers are PM localized and unlikely to reflect any vesicularization or internalization of SOAR1. These results are remarkable in revealing that one single point mutation within the SOAR1 dimer gives rise to a profound alteration in its PM distribution. Such cross-linking is supported by recent studies revealing ordered arrays of Orai1 channels and STIM1 proteins visualized at ER–PM junctions by electron microscopy after store depletion (36). In that study, Orai1 channel center-to-center distances were ∼15 nm. Orai channel hexamers are ∼8 nm across (29) and the SOAR dimer width is ∼6 nm (15), thus the theoretical distance between centers would be ∼14 nm, and is in good agreement with the EM measurements. A circular cluster with a 200-nm diameter would theoretically have 136 Orai1 channels if they were 15 nm center to center.

Although compelling, the clustering images obtained (Fig. 1 *C* and *D*) were for the YFP–SOAR1 dimer alone. We sought to obtain direct evidence that SOAR1 was clustering Orai1 channels; however, the Orai1–His molecule obviously could not be imaged directly. Thus, we undertook immunofluorescence staining analysis using both a YFP antibody to detect YFP–SOAR dimers, and a well-characterized Orai1 antibody (Sigma) to detect Orai1–His. Confocal immunofluorescence images of HEK Orai1–His cells expressing YFP-S-S (Fig. 1E) revealed obvious and almost entirely overlapping clustering of both the SOAR1 dimer and Orai1 channel. Clustering was particularly evident on the lower PM surface of cells. The images in Fig. 1E, *Lower Right* reveal a second cell that expresses only Orai1–His (not YFP-S-S) and shows no visible clustering. Using HEK Orai1–His cells expressing instead, YFP-S_H-S, identical immunofluorescence imaging revealed overlap of Orai1 and SOAR but little observable clustering, especially evident in the middle cell layer in which the cell edge enhances PM fluorescence (Fig. 1F). To eliminate any possible role of the His tag

in Orai1 clustering, we observed the same SOAR-dependent clustering in HEK cells stably expressing HA-tagged Orai1 with YFP-S-S, but not with YFP-S_H-S (*SI Appendix*, Fig. S2).

Overall, the results provide unique in vivo evidence that Orai1 channels are cross-linked by the active SOAR1 fragment of the STIM1 protein. We reveal that the unimolecular interaction between the SOAR dimer and Orai1 is key to this cross-linking of Orai1 channels. The F394H point mutation in just one SOAR subunit in the dimer is sufficient to block clustering (*SI Appendix*, Fig. S1C). An earlier chromatographic analysis of purified His-tagged Orai1 protein from cells coexpressing the STIM1 CAD fragment (similar to SOAR), revealed CAD–Orai1 complexes within which single-particle electron microscopy revealed CAD–Orai1 clusters (9). This in vitro visual evidence for clusters provides strong independent support for our in vivo imaging of SOAR-mediated Orai1 clustering.

Mobility of SOAR-Induced Cross-Linked Orai1 Channels. The data above reveal that the Orai1 channel activating moiety within STIM1, the SOAR1 dimer, is able to cross-link Orai1 channels by virtue of its two binding sites. Important to assess was the mobility of the SOAR–Orai1 complex and whether this correlates with the observed clustering. Mobility was assessed by fluorescence recovery after photobleaching (FRAP) analysis. Initially, we determined effects of the single F394H mutation in the SOAR1 dimer which prevents clustering (Fig. 1 and *SI Appendix*, Fig. S1C). We compared FRAP measurements for YFP-S-S and YFP-S_H-S expressed in HEK Orai1–His cells. The data reveal a major difference in the diffusional characteristics of YFP fluorescence for the two species (Fig. 2A and *SI Appendix*, Fig. S3 *A* and *B*). For YFP-S_H-S, fluorescence recovery in the bleached area reached almost 80%, and only 20% remained excluded from recovery as the immobile fraction. In contrast, with YFP-S-S, this immobile fraction was almost 60% of the fluorescence before bleaching (Fig. 2B). This large fraction of immobile species for YFP-S-S correlates well with the large visible clusters observed when expressed with Orai1–His (Fig. 1). Such clusters would not be expected to easily diffuse. Moreover, the rate of recovery of those fluorescent species that are able to diffuse into the bleached area was also substantially different between YFP-S-S and YFP-S_H-S. Thus, the diffusion coefficient (D) for YFP-S_H-S was more than double that of YFP-S-S (Fig. 2C). This indicates that even for the mobile fraction of YFP-S-S, there is a substantial increase in the size of the diffusing species (doubling of D suggests an approximately eightfold increase in size). Our FRAP image measurements were restricted to the PM and reflect movement only of SOAR1 dimer–Orai1 complexes since without Orai1, SOAR1 dimers are exclusively cytosolic (17). We revealed earlier that SOAR dimers do not undergo any direct interaction to form larger species (17, 18). In further studies, we compared FRAP for YFP-S-S and YFP-S_H-S using HEK Orai–CFP cells in which clustering between Orai1 channels is sterically prevented (*SI Appendix*, Fig. S1A). In this case, the immobile fraction for both YFP-S-S and YFP-S_H-S were similarly low (Fig. 2 *D* and *E* and *SI Appendix*, Fig. S3 *D* and *E*), around 20%, and there was no measurable difference in the D values (Fig. 2F). This provides important evidence that the diffusional characteristics are directly dependent on the ability of Orai1 to undergo clustering by SOAR dimer-induced cross-linking. Indeed, the profound changes in visible clustering, immobility, and diffusion rates as a result of the single F394H point mutation in the SOAR dimer, provide compelling evidence for cross-linking of Orai1 channels by the active site of STIM1.

Function of Orai1 Channels Cross-Linked by SOAR. We extended our comparative analysis of the two SOAR1 dimer species to examine functional activation of Orai1 channels by measuring Ca^{2+} release-activated Ca^{2+} current (I_{CRAC}). Our previous work
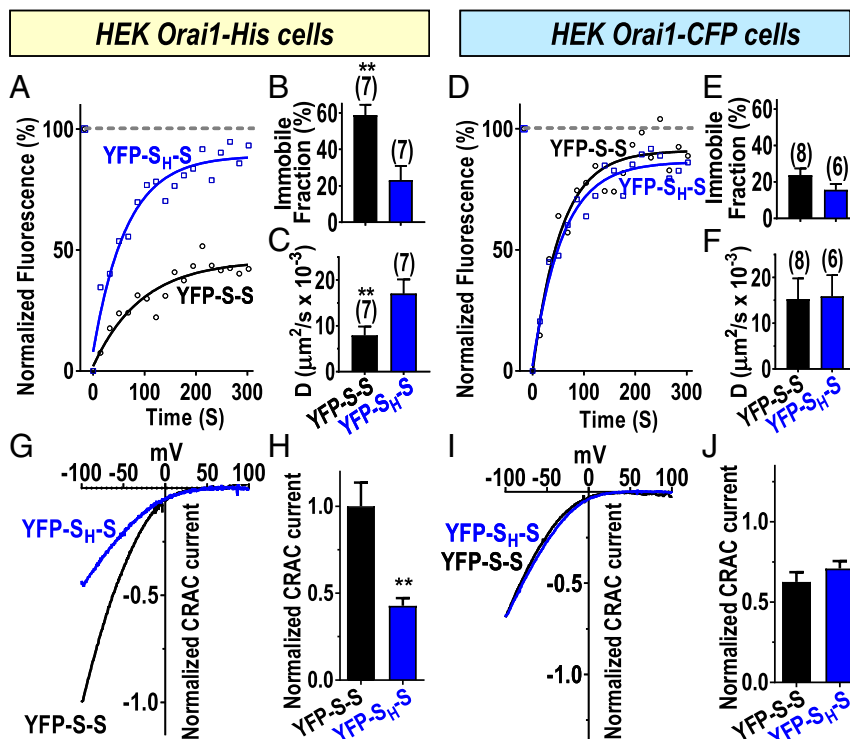
Fig. 2. Changes in channel mobility and function resulting from SOAR dimer-induced cross-linking of Orai1 channels. (*A–F*) Measurement of fluorescence recovery after photobleaching (FRAP) to assess diffusional characteristics. (*A–C*) Using stable HEK Orai1–His cells, YFP-S-S or YFP-S_H-S were expressed and fluorescence compared with prebleached levels (100%). After bleaching (8 s), fluorescence recovery was measured at 15-s intervals (*A*), and data fit to a one-phase exponential association equation to obtain diffusion coefficient (*D*) and immobile fraction. (*B*) Summary of immobile faction data derived from expression of YFP-S-S ($58.9 \pm 5.6\%$; $n = 7$ cells) or YFP-S_H-S ($23.2 \pm 7.7\%$; $n = 7$ cells). (*C*) Diffusion coefficients derived for YFP-S-S (7.9 ± 1.9 $\mu m^2/s \times 10^{-3}$; $n = 7$ cells) or YFP-S_H-S (17.1 ± 3.0 $\mu m^2/s \times 10^{-3}$; $n = 7$ cells). (*D–F*) Results obtained as in *A–C* except using HEK Orai1–CFP cells. (*E*) Summary of immobile fraction derived for YFP-S-S ($23.7 \pm 3.6\%$; $n = 8$ cells) or YFP-SH-S ($15.7 \pm 3.2\%$; $n = 6$ cells). (*F*) Diffusion coefficients derived for YFP-S-S (15.3 ± 4.5 $\mu m^2/s \times 10^{-3}$, $n = 8$ cells) or for YFP-S_H-S (15.9 ± 4.6 $\mu m^2/s \times 10^{-3}$; $n = 6$ cells). (*G*) Comparison of I_{CRAC} normalized to YFP intensity measured in stable HEK Orai1–His cells expressing either YFP-S-S or YFP-S_H-S. (*H*) Summary of peak currents generated in HEK Orai–His cells by YFP-S-S and YFP-S_H-S. Currents are normalized to YFP intensity and expressed as a fraction of the mean current (normalized I_{CRAC}) measured with YFP-S-S in HEK Orai1–His cells. The value for YFP-S-S is 1.00 ± 0.14 ($n = 12$ cells), and for YFP-S_H-S is 0.43 ± 0.04 ($n = 15$ cells). (*I*) Comparison of YFP-normalized I_{CRAC} measured in stable HEK Orai1–CFP cells expressing either YFP-S-S or YFP-S_H-S. (*J*) Summary of peak currents generated in HEK Orai–CFP cells by YFP-S-S and YFP-S_H-S. Currents are normalized to YFP intensity and expressed as a fraction of the mean current (normalized I_{CRAC}) measured with YFP-S-S in Orai1–His cells. The value for YFP-S-S is 0.62 ± 0.06 ($n = 15$ cells) and for YFP-S_H-S, 0.71 ± 0.05 ($n = 14$ cells). Representative traces are shown for *A, D, G,* and *I,* and summary data include means $\pm$ SEM for the number of cells shown. Representative FRAP traces are from three independent experiments; current traces are representative of four independent experiments. All data are presented as means $\pm$ SEM. **$P < 0.01$.

revealed that each SOAR1 monomer within a SOAR1 dimer is capable of independently inducing Orai1 channel activation through a unimolecular coupling mechanism (17). Now, using HEK Orai1–His cells, which permit cross-linking, we needed to determine whether SOAR1 dimers would induce activation of both of the channels they cross-link. The ability of SOAR1 dimers to cross-link Orai1 channels would be expected to result in a considerably larger current, since each SOAR1 dimer would be capable of interacting with and activating two separate Orai1 channel hexamers. We therefore measured I_{CRAC} in stable HEK Orai1–His cells, comparing the action of YFP-S-S and YFP-S_H-S (Fig. 2 *G* and *H*). In these experiments, we took care to relate the current density to the actual expression of each YFP–SOAR dimer. For this, we ensured that Orai1–His was expressed in excess over YFP–SOAR dimers so that Orai1 current density would be dependent on how many functional SOAR units were present (*SI Appendix*, Fig. S4 *A–I*). The results revealed that I_{CRAC} activated by the YFP-S-S homodimer was substantially greater (2.3-fold) than that measured in response to the YFP-S_H-S heterodimer (Fig. 2 *G* and *H*). The model shown in *SI Appendix*, Fig. S5 depicts a possible coupling pattern for each SOAR1 dimer construct. With a 2:1 ratio of Orai1:SOAR1 dimer, the YFP-S-S homodimer could maximally activate 70% of

the channels present (*SI Appendix*, Fig. S5*A*). In contrast, the YFP-S_H-S heterodimer would activate far fewer channels if it randomly associated with Orai1 channels (*SI Appendix, Fig. S5B*). Statistically, only 2% of Orai1 channels would have a full complement of six attached SOAR1 dimers, whereas 9% would have five and 24% would have four attached SOAR1 dimers (*SI Appendix, Fig. S5C*). Our recent assessment of Orai1 channel concatenated hexamers containing one or more pore-dead monomers (E106A) revealed that less than the full complement of functional hexamers severely reduces channel activity (31). Similar results were described for the inclusion of one or more STIM1 binding-defective monomers (L273D) in Orai1 channel concatenated hexamers (32). From these studies, we would estimate that the random association of YFP-S_H-S heterodimers with Orai1 channels would lead to only 10–15% of channel activity, as described in *SI Appendix*, Fig. S5*C*. Therefore, the observation that the YFP-S_H-S heterodimer has 43% of the activity of the YFP-S-S homodimer is intriguing and suggests that the association of SOAR units with Orai1 channels is strongly cooperative, a result that clearly warrants further investigation.

A further important control experiment was to compare Orai1–His channel activation when YFP-S-S or YFP-S_H-S were expressed in excess over Orai1–His. In this case, we observed

that the level of CRAC current induced by YFP-S-S was the same as that induced by YFP-S$_H$-S, again taking care to normalize observed current to the actual expression of each SOAR dimer (*SI Appendix*, Fig. S6 *A–D*). The model in *SI Appendix*, Fig. S6 *E and F* shows that under conditions in which each SOAR dimer was expressed in excess over Orai1–His, the channels would be expected to be fully and equally activated. This result is important in revealing that the YFP-S$_H$-S construct does not have any defect in Orai1 channel activation compared with YFP-S-S, other than its inability to cross-link adjacent channels to form clusters.

We also compared current generated by YFP-S-S and YFP-S$_H$-S expressed in HEK Orai1–CFP cells, again under conditions of excess Orai1. In this case, there was again no significant difference in the current generated by YFP-S-S and YFP-S$_H$-S (Fig. 2 *I* and *J*). This result is the same as we published in our previous work (17). However, at that time we did not know that cross-linking of Orai1 channels by SOAR1 was prevented by the bulky CFP group on Orai1. The unimolecular coupling model (17) predicts that, without the possibility of clustering, it makes no difference whether we express YFP-S-S or YFP-S$_H$-S, since either of them can only bind to a single Orai1 hexamer (*SI Appendix*, Fig. S5B). Thus, the result with HEK Orai1–CFP provides strong supporting evidence for the cross-linking of Orai1 channels.

Overall, the results on mobility and function provide important information that substantiate and extend the conclusions from Fig. 1 that reveal Orai1 clustering mediated by the SOAR dimer. The increased channel function provides further evidence that the SOAR dimer preferentially interacts through unimolecular interactions with two different hexameric Orai1 channels as opposed to a bimolecular interaction with two adjacent Orai1 subunits within a single hexamer, as previously proposed (19–22). Our studies continued to examine how cross-linking between channels may be controlled naturally, and what significance it may have in Ca^{2+} signal generation.

Function of SOAR from the STIM2 Splice Variant, STIM2.1. The widely expressed STIM2 protein differs from STIM1 in being more sensitive to ER Ca^{2+} store depletion (37), undergoing slower activation after depletion (38), and having a weaker efficacy for Orai1 channel activation (23). The latter is due to a lysine (L485) in the SOAR sequence of STIM2 replacing the functionally critical phenylalanine (F394) within the STIM1 SOAR sequence (23). Recent reports described an interesting naturally occurring splice variant of STIM2, STIM2.1 (or STIM2β) (27, 28). This variant is derived from alternative splicing of the highly conserved exon 9 in STIM2, resulting in the insertion of eight amino acids in the SOAR domain of STIM2, close to the critical Orai1-interacting domain (*SI Appendix*, Fig. S7 *A and B*) (27, 28). The STIM2.1 variant was reported to be devoid of Orai1-binding activity and was suggested to function as a negative regulator of SOCE. Certainly, the STIM2.1 splice variant is widely expressed (27, 28) and control of its appearance is believed to play an important role in the maintenance of naïve T cells (27), as well as regulating muscle and neural cell development through altered Ca^{2+} signaling (28). However, despite its potentially important role in regulating SOCE, the mechanism(s) by which such inhibitory effects are mediated by STIM2.1 is not well characterized.

We considered whether the Orai1 coupling defect of the STIM2.1 variant might represent a physiologically expressed STIM protein variant equivalent in function to the F394H mutation in STIM1 that is defective in Orai1 interaction. In studies to assess this, we initially compared the function of the full-length STIM proteins, STIM1, STIM1–F394H, and STIM2.1, as well as the SOAR units derived from each isoform. As shown in Fig. 3A using HEK Orai1–CFP cells, STIM1 induced typical I_{CRAC} following passive store depletion and application of Ca^{2+} to the external solution. Subsequent addition of 50 μM 2-aminoethoxydiphenyl borate (2-APB) caused a typical biphasic

response (39), with transient activation followed by blockade of this current. STIM1–F394H yielded no current, but 2-APB rapidly activated then inhibited I_{CRAC}. STIM2.1 gave no current and 2-APB did not induce any further effect. Using the isolated SOAR units from each STIM protein, FRET measurements revealed a high basal FRET between YFP–SOAR1 and Orai1–CFP (Fig. 3 *B* and *C*). The basal FRET with Orai1–CFP for YFP–SOAR1–F394H and YFP–SOAR2.1 were considerably lower, indicating that both these SOAR units had much lower affinity for Orai1 than YFP–SOAR1. The 2-APB slightly enhanced the high FRET between SOAR1 and Orai1–CFP. However, 2-APB greatly increased the FRET between SOAR1–F394H and Orai1–CFP. In contrast, the low basal FRET between SOAR2.1 and Orai1–CFP was barely altered by 2-APB. We also compared the action of the SOAR units on Ca^{2+} entry (Fig. 3D), now using HEK Orai–His cells in case the prevention of Orai1 clustering might influence the action of SOAR units.
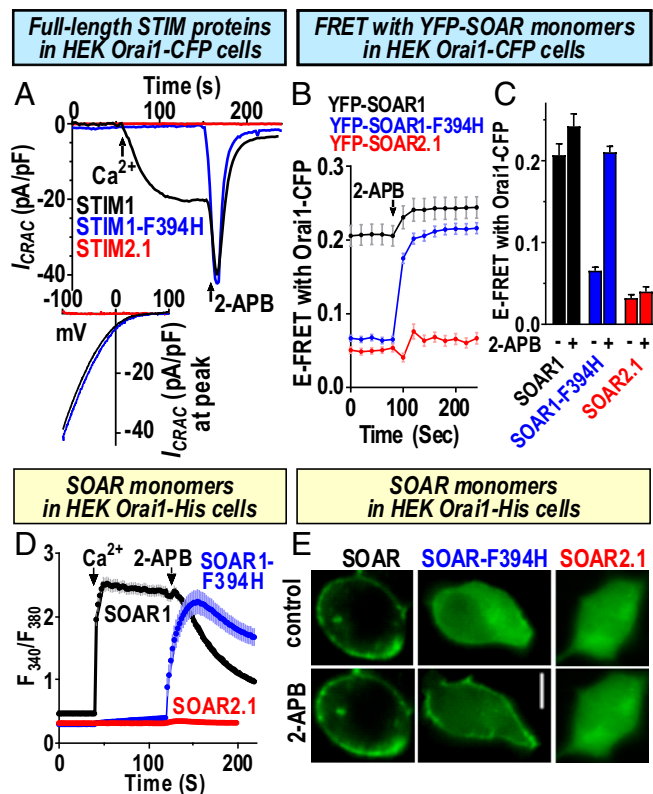

Fig. 3. Comparison of the function of full-length STIM1, STIM1–F394H, and STIM2.1, and the SOAR fragments derived therefrom. (*A*) I_{CRAC} measurements in HEK Orai1–CFP cells transiently expressing either STIM1, STIM–F394H, or STIM2.1. Stores were passively depleted with 10 mM BAPTA in the pipette and 20 mM Ca^{2+} bath solution, and 50 μM 2-APB was added as shown. (*B*) E-FRET was measured in HEK Orai1–CFP cells expressing either YFP–SOAR1, YFP–SOAR1–F394H, or YFP–SOAR2.1. Basal values and values after 50 μM 2-APB addition were obtained and summarized in *C*. (*C*) SOAR1 (basal, 0.207 ± 0.014; after 2-APB, 0.242 ± 0.015; *n* = 42 cells), YFP–SOAR1–F394H (basal, 0.066 ± 0.004; after 2-APB, 0.210 ± 0.007; *n* = 43 cells), and YFP–SOAR2.1 (basal, 0.032 ± 0.005; after 2-APB, 0.040 ± 0.006; *n* = 34 cells). Summary data from three separate transfections are shown (means ± SEM). (*D*) Ca^{2+} imaging in fura2-loaded HEK Orai1–His cells expressing YFP–SOAR1, YFP–SOAR1–F394H, or YFP–SOAR2.1. Constitutive Ca^{2+} entry was measured following addition of 1 mM extracellular Ca^{2+} and 50 μM 2-APB as shown. (*E*) Fluorescence images showing the distribution of YFP–SOAR1, YFP–SOAR1–F394H, or YFP–SOAR2.1 expressed in HEK Oria1–His cells, either before (*Top*) or after (*Bottom*) addition of 50 μM 2-APB. (Scale bar, 10 μm.) Representative traces and images are from three independent experiments; data are means ± SEM.

Clearly, we observed the same distinct effects of 2-APB which restored the action of SOAR1–F394H on Ca^{2+} entry but not that of SOAR2.1. Earlier, we revealed that the reversing effect of 2-APB on the function of SOAR1–F394H was due to a 2-APB–induced physical coupling between SOAR1–F394H and Orai1. As shown in Fig. 3E, SOAR1 was attached to PM Orai1 before 2-APB addition. The 2-APB considerably enhanced the attachment of SOAR1–F394H to Orai1, whereas cytosolic SOAR2.1 remained entirely cytosolic even after 2-APB. These results indicate that although both SOAR1–F394H and SOAR2.1 have a complete Orai1-binding defect, the SOAR2.1-binding defect was perhaps more severe than that of SOAR1–F394H since it could not be reversed by 2-APB.

STIM2.1 Prevents Cross-Linking but Not the Function of Orai1 Channels.
Important to ascertain was whether the dimer formed between STIM1 and STIM2.1 was able to still interact with the Orai1 channel, and more importantly, whether such a heterodimer was able to successfully gate the channel. To answer this, we con-structed new heterodimers of SOAR1 and SOAR2.1, as well as the SOAR2.1 homodimer (*SI Appendix,* Fig. S7C). Initially, we examined the ability of the SOAR dimers to interact with Orai1 by imaging. Clearly, both YFP-S-S and YFP-S$_{2.1}$-S showed avid as-sociation and complete overlap when coexpressed with Orai1–CFP (Fig. 4 A and B). In contrast, the YFP-S$_{2.1}$-S$_{2.1}$ SOAR dimer had no association with Orai1–CFP (Fig. 4C). We also analyzed FRET between each of the YFP-tagged SOAR dimers and Orai1–CFP and observed that the YFP-S-S and the YFP-S$_{2.1}$-S constructs had almost identical high levels of FRET with Orai1–CFP, whereas the YFP-S$_{2.1}$-S$_{2.1}$ dimer had negligible FRET (Fig. 4D). These imaging and FRET results reveal that the strong interaction of SOAR1 with Orai1 was not compromised by having one SOAR1 monomer replaced by SOAR2.1 and are consistent with the unimolecular coupling model (17). Important to examine was whether the SOAR2.1 moiety within the SOAR dimer would alter cross-linking of Orai1 channels. For this we again employed the HEK Orai1–His cells. The clustered distribution of the YFP-S-S (Fig. 4E) clearly contrasted with the smooth distribution of YFP-S$_{2.1}$-S cells
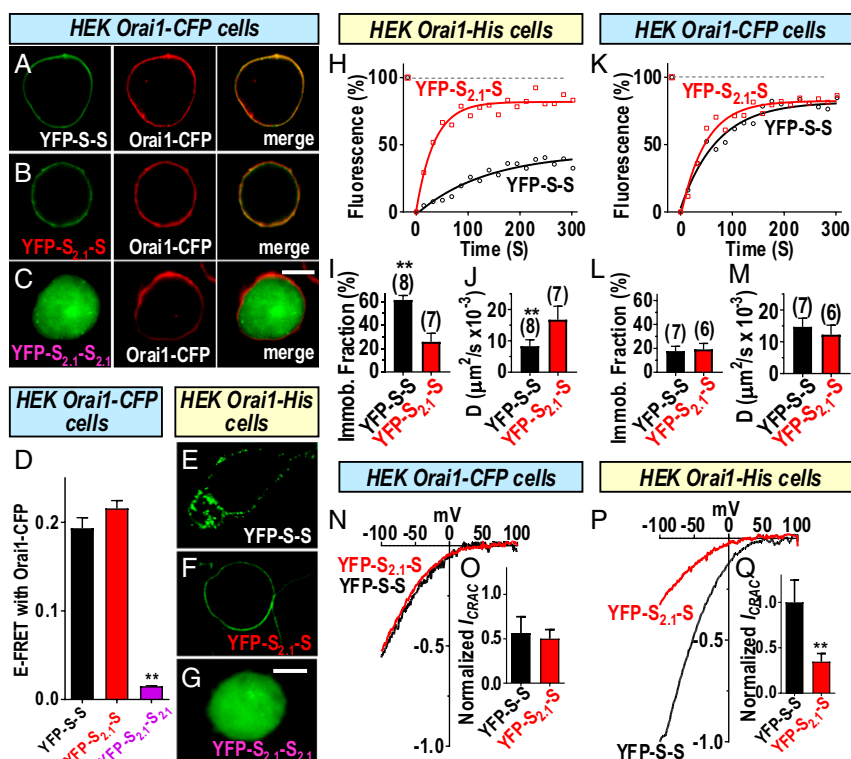

Fig. 4. The SOAR2.1 heterodimer blocks cross-linking but not the functional coupling of Orai1 channels. Experiments compared the distribution and actions of the YFP-tagged concatenated SOAR heterodimer (YFP-S$_{2.1}$-S) and homodimer (YFP-S$_{2.1}$-S$_{2.1}$) constructs (*SI Appendix,* Fig. S7) with the wild type of SOAR homodimer (YFP-S-S). Fluorescence images of YFP-S-S (A) or YFP-S$_{2.1}$-S (B) expressed in HEK Orai1–CFP cells, revealing close overlap of YFP–SOAR and Orai1–CFP in the merged images. In contrast, YFP-S$_{2.1}$-S$_{2.1}$ (C) does not associate with Orai1. (D) FRET between YFP–SOAR dimers expressed in HEK Orai1–CFP cells shows strong FRET between Orai1–CFP and YFP-S-S (0.193 ± 0.012; n = 21 cells) or YFP-S$_{2.1}$-S (0.216 ± 0.009; n = 15 cells), but almost no FRET with YFP-S$_{2.1}$-S$_{2.1}$ (0.015 ± 0.001; n = 16 cells). YFP-S-S expressed in HEK Orai1–His cells is clearly clustered (E), whereas YFP-S$_{2.1}$-S has a smooth nonclustered distribution on the PM (F), and YFP-S$_{2.1}$-S$_{2.1}$ does not associate with Orai1 in the PM (G). (H–J) FRAP measurements for YFP-S-S and YFP-S$_{2.1}$-S dimers expressed in HEK Orai1–His cells. (H) Time dependence of fluorescence compared with levels before the 8-s bleaching period (100%). (I) Summary of fraction of immobile fluorescence from FRAP data for YFP-S-S (25.7 ± 7.3%; n = 7 cells) or YFP-S$_{2.1}$-S (61.4 ± 3.8%; n = 8 cells). (J) Summary of diffusion coefficient (D) measurements derived from FRAP data for YFP-S-S (8.3 ± 2.0 μm^2/s ×10^{-3}; n = 8 cells) or YFP-S$_{2.1}$-S (16.8 ± 4.3 μm^2/s ×10^{-3}; n = 7 cells). (K–M) FRAP measurements for YFP-S-S and YFP-S$_{2.1}$-S dimers expressed in HEK Orai1–CFP cells. (K) Time dependence of fluorescence compared with levels before the 8-s bleaching period (100%). (L) Summary of fraction of immobile fluorescence from FRAP data for YFP-S-S (17.7 ± 4.0%; n = 7 cells) or YFP-S$_{2.1}$-S (19.2 ± 5.0%; n = 6 cells). (M) Summary of diffusion coefficient (D) measurements derived from FRAP data for YFP-S-S (14.7 ± 2.7 μm^2/s ×10^{-3}; n = 7 cells), or YFP-S$_{2.1}$-S (12.2 ± 3.0 μm^2/s ×10^{-3}; n = 6 cells). (N) Comparison of I_{CRAC} measured in HEK Orai1–CFP cells expressing either YFP-S-S or YFP-S$_H$-S. (O) Summary of peak currents generated in HEK Orai–CFP cells by YFP-S-S (0.56 ± 0.19; n = 6) or YFP-S$_{2.1}$-S (0.50 ± 0.10; n = 7 cells). (P) I_{CRAC} in HEK Orai1–His cells expressing either YFP-S-S or YFP-S$_{2.1}$-S. (Q) Summary of peak currents generated in HEK Orai–His cells by YFP-S-S (1.00 ± 0.25; n = 15 cells) or YFP-S$_{2.1}$-S (0.35 ± 0.09; n = 6 cells). In each case, currents were normalized to YFP intensity and expressed as a fraction of the mean current (normalized I_{CRAC}) measured with YFP-S-S in Orai1–His cells. Representative traces from three independent experiments are shown for H, K, N, and P; summary data are means ± SEM for cell numbers shown. **P < 0.001. [Scale bars, C and G, 10 μm (also apply to A and B and E and F, respectively).]

(Fig. 4*F*), whereas the YFP-S$_{2.1}$-S$_{2.1}$ remained cytosolic (Fig. 4*G*). The results indicate that the single SOAR2.1 moiety in the SOAR dimer does prevent cross-linking of Orai channels. To further assess the action of SOAR2.1 on cross-linking, we undertook comparative FRAP analyses on the YFP–SOAR dimers. Expressed in HEK Orai1–His cells, the immobilized fraction of YFP-S$_{2.1}$-S was ~20%, whereas that for YFP-S-S was 60% (Fig. 4 *H* and *I*). Moreover, the diffusion coefficient (*D*) for the YFP-S-S reappearing in the bleached area was less than half that for YFP-S$_{2.1}$-S (Fig. 4*J*). In contrast, expressed instead in the HEK Orai1–CFP cells in which clustering is sterically prevented, the same two SOAR dimers had a similar small immobile fraction (~20%) (Fig. 4 *K* and *L*), and diffused into the bleached area at a similar fast rate (Fig. 4*M*). In summary, the imaging, FRET, and FRAP results provide a consistent picture in which SOAR dimers can mediate clustering between Orai channels. This clustering is prevented either by a single non Orai1-binding monomer in the SOAR dimer or by the presence of a bulky CFP moiety on Orai1 monomers. Thus, the SOAR unit within the STIM2.1 splice variant is highly equivalent to the SOAR–F394H mutant described above.

An important question arising is whether the YFP-S$_{2.1}$-S heterodimeric SOAR unit is functional in activating the Orai1 channel. Rana et al. (28) recently suggested that the eight additional amino acid segment in STIM2.1 might actively alter the Orai1 channel through a sequence-specific allosteric interaction with Orai1. They showed that STIM2.1 delayed STIM1-induced activation of Orai1. They also predicted that STIM2.1 would have a dominant effect and that a heterodimer between STIM1 and STIM2.1 would be inactive. However, although they constructed a heterodimer of CAD1 and CAD2.1, no functional data were presented on this heterodimer. We therefore compared Orai1 channel activation by the YFP-S-S homodimer and the YFP-S$_{2.1}$-S heterodimer of SOAR, carefully normalizing current to the expression of each SOAR dimer. Expressed in HEK Orai1–CFP cells we observed almost identical CRAC current with the two dimers (Fig. 4*N*). Thus, the YFP-S$_{2.1}$-S heterodimer clearly does function to couple with and activate Orai1 channels, providing proof that the SOAR2.1 moiety does not actively block function of the wild-type SOAR1 within the same dimer. Since the HEK Orai1–CFP cells do not permit clustering, we extended our study to examine the action of both dimers within HEK Orai1–His cells in which cross-linking can occur. We observed a substantial (threefold) increase in the CRAC current with the YFP-S-S homodimer compared with that mediated by the YFP-S$_{2.1}$-S heterodimer (Fig. 4 *P* and *Q*). We conclude from these results that, while the YFP-S$_{2.1}$-S heterodimer is functional in activating the Orai1 channel, it is defective in cross-linking the channel and hence is analogous in function to the YFP-S$_H$-S heterodimer. Thus, the model described above and shown in *SI Appendix*, Fig. S5 for the YFP-S$_H$-S again applies. Without the ability of channels to be cross-linked, the YFP-S$_{2.1}$-S heterodimer results in substantially less (35%) channel activation. However, this number is again significantly above the theoretical value calculated for random interactions of heterodimers and suggests that the interaction of the YFP-S$_{2.1}$-S heterodimer is undergoing a similar positive cooperativity in binding to Orai1.

These results provide a strong functional correlate to the imaging, FRET and FRAP evidence that cross-linking of Orai1 channels is prevented by the SOAR2.1 monomer within the SOAR heterodimer. Importantly, the Orai1 channel activation data in Fig. 4*N* reveal that the added eight-amino acid segment in the SOAR2.1 unit within the heterodimer with SOAR1, does not prevent the heterodimer from assembling into a functional dimer, a result that contradicts the earlier prediction that such a heterodimer would not activate Orai1 channels (28). Although the structural model (*SI Appendix*, Fig. S7*B*) depicts a simple unstructured "blebbed" eight-residue insert similar to that suggested earlier (28), more likely the insert is helical and extends

the SOAR α1 helix by two turns (27). Potentially, such an extended helical structure could have inflicted a more substantial alteration in the SOAR structure that might be expected to alter the entire SOAR dimeric structure and prevent any gating interaction with the Orai1 channel. Indeed, the inability of 2-APB to restore function to STIM2.1 or SOAR2.1 (Fig. 3) suggested that the defect in SOAR2.1 was more substantial than that in SOAR1–F394H. Surprisingly, however, our results reveal that the SOAR2.1 insert is functionally equivalent to the SOAR–F394H point mutation, and simply prevents only one half of the heterodimer from interacting with Orai1, presumably without altering the intermolecular interactions at the interface between SOAR monomers.

STIM2.1 Modulates Ca^{2+} Oscillations Through Impaired Orai1 Channel Cross-Linking. Our results reveal a remarkable ability of the SOAR active site in STIM1 to mediate cross-linking between Orai1 channels. The SOAR unit from the widely expressed STIM2.1 variant impedes this clustering, although, surprisingly, it does not block the action of STIM1 as a heterodimer. Important to assess these actions might modulate the generation of physiological Ca^{2+} signals. We therefore examined how full-length STIM2.1 coexpressed with STIM1 would alter receptor-induced Ca^{2+} signals. To eliminate interference from endogenous STIM proteins, we utilized HEK cells in which endogenous STIM1 and STIM2 expression was eliminated using CRISPR/Cas9 gene editing (*SI Appendix*, Fig. S8). We measured receptor-induced Ca^{2+} signals in the CRISPR-derived HEK S1S2–dKO cells expressing either STIM1 alone or the same level of STIM1 coexpressed together with STIM2.1 (*SI Appendix*, Fig. S9 *A–D*). To mimic the probable molar ratio of STIM1 and STIM2.1 (discussed below), we analyzed cells expressing a ratio of STIM1:STIM2.1 of 5:1 (*SI Appendix*, Fig. S9 *E–I*). Initially we examined the effects of STIM1 and STIM2.1 coexpression on the sustained oscillatory responses to a physiological dose of phospholipase C (PLC)-coupled agonist. In cells expressing STIM1 alone, baseline oscillations in response to 3 μM carbachol (CCh) continued with a relatively stable frequency for 15 min (Fig. 5*A*). With the coexpression of STIM2.1, baseline oscillations were still observed, but decreased substantially in frequency with time (Fig. 5*B*). The data from many cells revealed that after 15 min, the presence of STIM2.1 with STIM1 had reduced the frequency of oscillations to one-third of those seen with STIM1 alone (Fig. 5*C*). We also examined the action of STIM1 and STIM2.1 expression on the dose dependence of oscillatory Ca^{2+} signals induced by carbachol. In cells expressing STIM1 alone, the response to increases in carbachol reveals an augmentation of Ca^{2+} oscillation frequency in the physiological (1–10 μM) range (Fig. 5*D*). At higher carbachol levels, oscillations are superseded by a continuous plateau of Ca^{2+}, likely caused by Ca^{2+} overload due to a combination of sustained Ca^{2+} release from stores and higher store-operated Ca^{2+} entry. At these higher stimulus levels, the number of cells showing oscillations is greatly decreased (Fig. 5*F*) and the frequency of Ca^{2+} oscillations that can be observed is substantially reduced (Fig. 5*G*). In contrast, coexpression of STIM2.1 and STIM1 results in an interesting protection against the refractoriness of Ca^{2+} responses seen with high agonist levels in cells expressing STIM1 alone (Fig. 5*E*). With both STIM proteins expressed, most of the cells retained clearly observable, sustained oscillations (Fig. 5*F*) with albeit slightly reduced frequency (Fig. 5*D*). In this case, it appears that the STIM2.1 coexpression has limited the excessive Ca^{2+} entry resulting from robust store depletion. We tested this explanation by examining responses to 100 μM CCh in either normal 1 mM extracellular Ca^{2+} or in 0.1 mM extracellular Ca^{2+} to reduce Ca^{2+} entry (*SI Appendix*, Fig. S10). Clearly, the decreased extracellular Ca^{2+} caused the plateau Ca^{2+} response to be converted to an oscillatory response in most cells. Thus, we conclude
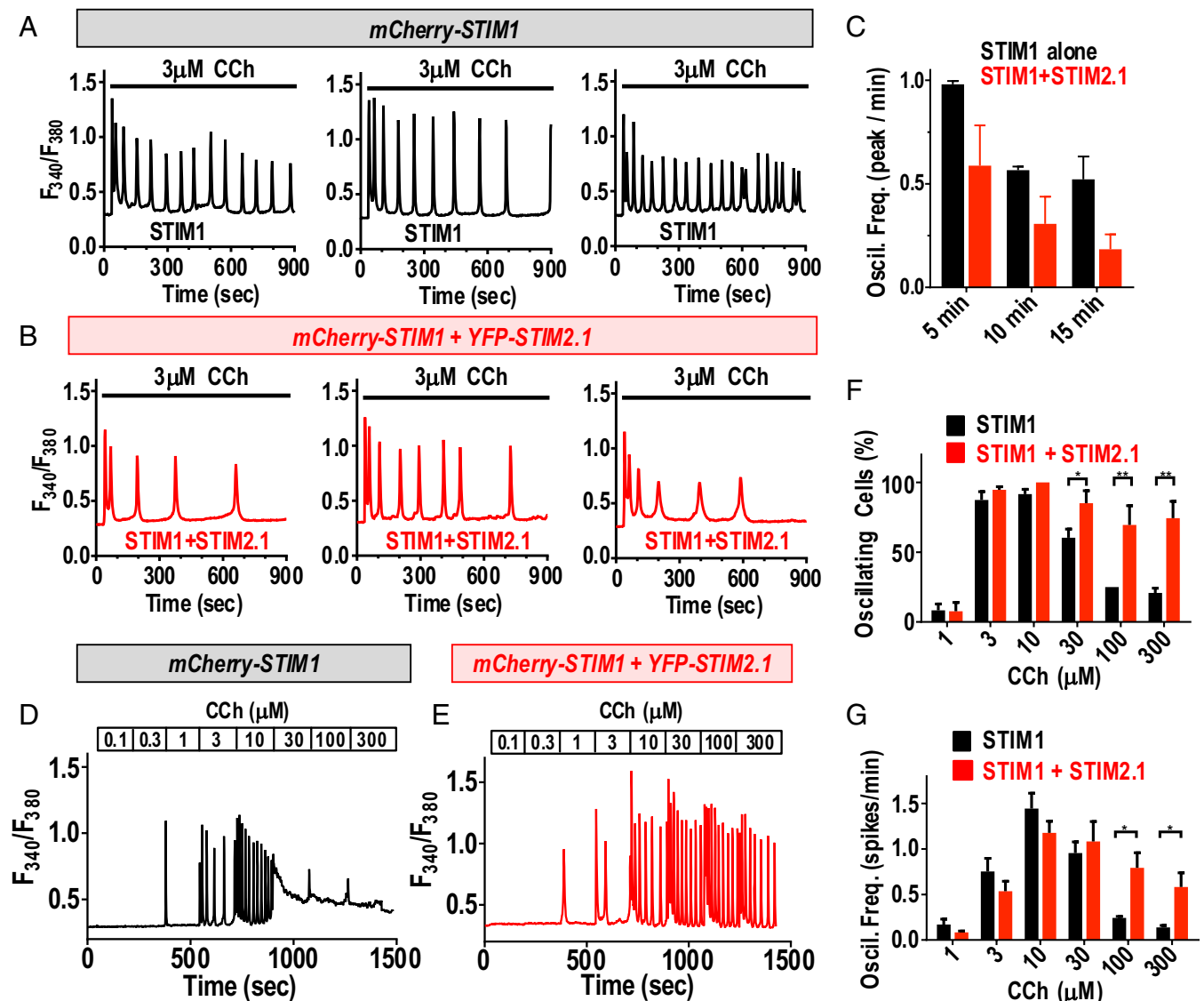
Fig. 5. Modulation of agonist-induced Ca^{2+} oscillations by STIM2.1. Ca^{2+} oscillatory responses to carbachol were measured in CRISPR-derived HEK cells devoid of endogenous STIM1 and STIM2 (HEK S1S2–dKO cells). (*A*) Representative Ca^{2+} responses to 3 μM carbachol measured in HEK S1S2–dKO cells transfected with mCherry–STIM1. (*B*) Ca^{2+} responses to 3 μM carbachol measured in HEK S1S2–dKO cells transfected with mCherry–STIM1 together with YFP–STIM2.1. (*C*) Summary data for the time dependence of oscillations in response to 3 μM carbachol in HEK S1S2–dKO cells expressing STIM1 alone (black; n = 35 cells) or STIM1 together with STIM2.1 (red; n = 44 cells). (*D* and *E*) Representative traces of Ca^{2+} oscillatory responses to a range of carbachol levels sequentially added to HEK S1S2–dKO expressing either mCherry–STIM1 alone (*D*) or mCherry–STIM1 together with YFP–STIM2.1 (*E*). (*F*) Summary data from multiple cells of the fraction of cells giving oscillatory responses at each carbachol concentration shown. (*G*) Summary from multiple cells of the frequency of Ca^{2+} oscillations observed in response to the range of carbachol. For both *F* and *G*, data are the summary from 66 cells expressing mCherry–STIM1 alone (black), and 52 cells expressing mCherry–STIM1 together with YFP–STIM2.1 (red), in each case derived from three separate transfections. For all experiments shown, the level of mCherry–STIM1 expression was the same, both in the presence or absence of YFP–STIM2.1 (*SI Appendix*, Fig. S9 *A–D*). In cells transfected with both mCherry–STIM1 and YFP–STIM2.1, the ratio of STIM1 to STIM2.1 was 5:1, as determined in *SI Appendix*, Fig. S9. Representative traces are from four independent experiments. Summary data shown are means ± SEM; *P < 0.01; **P < 0.001.

that the STIM2.1-mediated inhibition of Orai1 channel cross-linking has a protective effect and appears to avert Ca^{2+} entry overload. Overall, these results reveal that the coexpression of even a small fraction of STIM2.1 together with STIM1 results in a considerable alteration in Ca^{2+} signal generation, likely through limiting the degree of Ca^{2+} entry.

Concluding Remarks. The compact, highly conserved SOAR units from STIM proteins, self-assemble into dimers that undergo coupling and activation of Orai1 channels, closely recapitulating the function of full-length STIM proteins (8–10, 17, 23). Our recent evidence (7, 17, 40) militates strongly against an earlier

bimolecular coupling model for the STIM–Orai interaction (19–22). Instead, we reveal that while SOAR must be presented to Orai1 as a dimer, the SOAR monomer units within the SOAR dimer interact independently in a unimolecular mode with single Orai1 subunits (17). The ability to build concatenated SOAR dimers allowed us to examine specific heterodimers that cannot be constructed with full-length STIM proteins. Using these, we were able to identify cross-linking of Orai1 channels through high-resolution imaging, diffusional measurements, and assessment of functional stoichiometry.

The STIM-mediated cross-linking of Orai1 channels represents a unique functional paradigm for store-operated Ca^{2+}

signaling. Our studies indicate that Orai1 channel cross-linking within ER–PM junctions has important consequences in Ca^{2+} signal generation. Until now, it has been assumed that the localization of STIM1 within ER–PM junctions results in passive "herding" of Orai1 channels within these junctions. Indeed, the theory that STIM1 undergoes a bimolecular interaction with two adjacent Orai1 subunits in a single Orai1 hexameric channel (19–22), precluded consideration of STIM-induced Orai1 channel cross-linking. Moreover, we reveal that bulky fluorescent tags on Orai1 sterically block Orai1 cross-linking, explaining why cross-linking was not previously recognized. The cross-linking we observe with SOAR dimers also explains the regularly spaced arrays of Orai1 and full-length STIM1 observed in ER–PM junctions of store-depleted cells by EM freeze fracture (36). Hence, the same unimolecular coupling and cross-linking of Orai1 channels mediated by SOAR dimers likely occurs during the coupling of full-length STIM1 with Orai1 channels within ER–PM junctions.

A model for the physiological role of STIM–Orai cross-linking in Ca^{2+} signal generation within the ER–PM junctional microenvironment, is shown in Fig. 6. The cross-linking likely increases the efficacy of channel activation, since each STIM protein activates twice the number of channels. Moreover, our results suggest strong cooperativity in the unimolecular interaction between SOAR1 and Orai1 which would further increase the efficiency of activation. Thus, cooperative cross-linking could substantially enhance the rate of channel activation by STIM1, and may also be important in assisting channel deactivation and dissociation from Orai1 following STIM1 refolding after store replenishment. Our results indicate that the enhanced efficacy of SOCE due to channel cross-linking is important in replenishing ER Ca^{2+}, necessary for sustaining agonist-induced Ca^{2+} oscillations mediated by ER Ca^{2+} release (Fig. 6A). Enhanced Ca^{2+} entry would also be important in mediating downstream SOCE "signature" responses (12, 41), including the activation of calcineurin and subsequent transcriptional control through nuclear factor of activated T cells (NFAT) (12, 41–45).

The actions of the widely expressed STIM2.1 splice variant described here underscore the significance of the cross-linked STIM1–Orai1 microenvironment in ER–PM junctions. While the SOAR2.1 homodimer cannot bind to Orai1, the SOAR1–SOAR2.1 heterodimer does bind, consistent with the unimolecular coupling model (17). This fits with recent colocalization and FRET studies, revealing that coexpressed full-length STIM1 and STIM2.1 do form heterodimers (28). Although STIM2.1 homodimers have no intrinsic ability to couple with or activate Orai1 (27, 28), under conditions of store emptying, colocalization studies revealed that STIM1–STIM2.1 heterodimers move into junctions and associate with Orai1 channels (28). However, in this study it was thought that such STIM1–STIM2.1 heterodimer complexes with Orai1, were inactive. In contrast, we show here that the SOAR1–SOAR2.1 heterodimer can cause full activation of Orai1 in HEK Orai1–CFP cells. This means that STIM2.1 does not simply displace or dominate the action of STIM1 by combining with it, as earlier suggested (28). Instead, STIM2.1 functions solely to prevent Orai1 channel cross-linking. In this way it is able to attenuate the increased efficiency conferred on Orai1 channel activation by STIM1-mediated cross-linking, as depicted in the model in Fig. 6B. The consequence of this STIM2.1-mediated limitation of cross-linking, is decreased SOCE, resulting in lowered store refilling, and the modulation of oscillatory Ca^{2+} signals. In addition, the decreased SOCE would result in lowered SOCE signature responses (SSRs), including the activation of calcineurin and NFAT (3).

In summary, our studies reveal the SOAR domains in STIM protein dimers containing two independent Orai1 binding sites, can cross-link Orai1 channels, resulting in clusters of considerable size, easily detected by imaging. The single point mutation
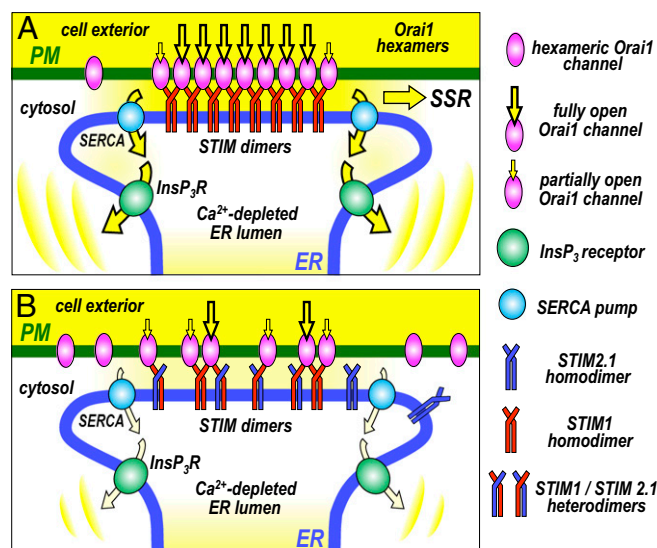

Fig. 6. Model for the cross-linking of Orai channels by STIM proteins and its physiological role in the generation of Ca^{2+} signals. (A) When STIM1 is the major STIM protein isoform present, the homodimers of STIM1 moving into ER–PM junctions are able to cross-link hexameric Orai1 channels, increasing the efficacy, rate, and density of Orai1 channel activation in junctions. This results in a maximal number of activated Orai1 channels mediating store-operated Ca^{2+} entry (SOCE) at the ER–PM junction. The larger SOCE allows efficient Ca^{2+} store refilling via sarco/endoplasmic reticulum Ca^{2+} ATPase (SERCA) Ca^{2+} pumps, which sustains the generation of oscillatory Ca^{2+} release signals mediated by inositol trisphosphate receptors ($InsP_3R$). The enhanced SOCE may also increase downstream SOCE signature responses (SSRs), for example, activation of calcineurin and NFAT. (B) When cells express the splice variant, STIM2.1 together with STIM1, heterodimers of STIM1 and STIM2.1 move into junctions, but can only undergo monomeric interactions with Orai1 channels. They are unable to cross-link Orai1 channels and hence prevent clustering. This results in lowered efficacy, rate, and density of Orai1 channel activation. The decreased SOCE results in lowered store refilling and the inability of cells to sustain the generation of oscillatory Ca^{2+} release signals. The decreased SOCE may also reduce SSR. Thus, STIM2.1 may act as a powerful regulator of SOCE. Note that STIM2.1 homodimers play no role; they cannot bind Orai1, nor can they directly influence cross-linking.

(F394H) or the eight-amino acid insert in SOAR2.1, in each case result in complete prevention of the observed cross-linking and clustering of Orai1 channels. Through its actions to prevent STIM1-mediated Orai1 channel cross-linking, STIM2.1 likely acts as a powerful regulator of SOCE. The observed inability to sustain Ca^{2+} oscillations and the protection of cells from Ca^{2+} overload are reflections of this role. Importantly, it should be recalled that STIM2 (and hence STIM2.1) has enhanced sensitivity to store emptying due to its altered EF hand-mediated Ca^{2+} sensing domain (46, 47). This means that at physiological PLC-coupled receptor agonist levels with minimal or modest store emptying, both STIM2 and STIM2.1 are preferentially activated and translocate into junctions. Indeed, by forming heterodimers, STIM2 is shown to promote recruitment of STIM1 into ER–PM junctions under low-agonist conditions with mild store depletion (48). STIM2 is ubiquitously expressed among cell types and is reported to exceed STIM1 in certain tissues, including brain, liver, heart, and dendritic cells (1, 3, 49). Relative to STIM2, the expression of STIM2.1 varies from 10% to 50%, depending on cell type (27). Our results reveal a considerable r effect of STIM2.1 when expressed at only 20% of STIM1. Given the preferential translocation of STIM2.1 into junctions under modest store-depletion conditions in which STIM1 is less activated, it is likely that STIM2.1 exerts a powerful effect on Ca^{2+} signals. Overall, our work reveals STIM-mediated cross-linking

       Zhou et al.

of Orai1 channels as a hitherto unrecognized functional paradigm that likely provides an organizational microenvironment within ER–PM junctions that has an important functional impact on Ca^{2+} signal generation.

Materials and Methods

Details of DNA constructs, generation of CRISPR/Cas9-derived knockout cell lines, cell culture, transfection conditions, Ca^{2+} measurements, FRET analysis, superresolution imaging, FRAP measurements, electrophysiology, Western analysis, structural modeling, and statistics are provided *SI Appendix, SI Materials and Methods*.

1. Soboloff J, Rothberg BS, Madesh M, Gill DL (2012) STIM proteins: Dynamic calcium signal transducers. *Nat Rev Mol Cell Biol* 13:549–565.
2. Gudlur A, Zhou Y, Hogan PG (2013) STIM-ORAI interactions that control the CRAC channel. *Curr Top Membr* 71:33–58.
3. Prakriya M, Lewis RS (2015) Store-operated calcium channels. *Physiol Rev* 95:1383–1436.
4. Shim AH, Tirado-Lee L, Prakriya M (2015) Structural and functional mechanisms of CRAC channel regulation. *J Mol Biol* 427:77–93.
5. Amcheslavsky A, et al. (2015) Molecular biophysics of Orai store-operated Ca2+ channels. *Biophys J* 108:237–246.
6. Derler I, Jardin I, Romanin C (2016) Molecular mechanisms of STIM/Orai communication. *Am J Physiol Cell Physiol* 310:C643–C662.
7. Zhou Y, et al. (2017) The STIM-Orai coupling interface and gating of the Orai1 channel. *Cell Calcium* 63:8–13.
8. Yuan JP, et al. (2009) SOAR and the polybasic STIM1 domains gate and regulate Orai channels. *Nat Cell Biol* 11:337–343.
9. Park CY, et al. (2009) STIM1 clusters and activates CRAC channels via direct binding of a cytosolic domain to Orai1. *Cell* 136:876–890.
10. Muik M, et al. (2009) A cytosolic homomerization and a modulatory domain within STIM1 C-terminus determine coupling to ORAI1 channels. *J Biol Chem* 284:8421–8426.
11. Kar P, Nelson C, Parekh AB (2012) CRAC channels drive digital activation and provide analog control and synergy to Ca$^{(2+)}$-dependent gene regulation. *Curr Biol* 22:242–247.
12. Zhou Y, Trebak M, Gill DL (2015) Calcium signals tune the fidelity of transcriptional responses. *Mol Cell* 58:197–199.
13. Rothberg BS, Wang Y, Gill DL (2013) Orai channel pore properties and gating by STIM: Implications from the Orai crystal structure. *Sci Signal* 6:pe9.
14. Covington ED, Wu MM, Lewis RS (2010) Essential role for the CRAC activation domain in store-dependent oligomerization of STIM1. *Mol Biol Cell* 21:1897–1907.
15. Yang X, Jin H, Cai X, Li S, Shen Y (2012) Structural and mechanistic insights into the activation of Stromal interaction molecule 1 (STIM1). *Proc Natl Acad Sci USA* 109:5657–5662.
16. Zhou Y, et al. (2013) Initial activation of STIM1, the regulator of store-operated calcium entry. *Nat Struct Mol Biol* 20:973–981.
17. Zhou Y, et al. (2015) STIM1 dimers undergo unimolecular coupling to activate Orai1 channels. *Nat Commun* 6:8395.
18. Ma G, et al. (2015) Inside-out Ca$^{(2+)}$ signalling prompted by STIM1 conformational switch. *Nat Commun* 6:7826.
19. Stathopulos PB, et al. (2013) STIM1/Orai1 coiled-coil interplay in the regulation of store-operated calcium entry. *Nat Commun* 4:2963.
20. Yen M, Lokteva LA, Lewis RS (2014) STIM1 binds to pairs of Orai1 subunits to open the CRAC channel. *Biophys J* 106:314a–315a.
21. Fahrner M, et al. (2014) A coiled-coil clamp controls both conformation and clustering of stromal interaction molecule 1 (STIM1). *J Biol Chem* 289:33231–33244.
22. Maus M, et al. (2015) Missense mutation in immunodeficient patients shows the multifunctional roles of coiled-coil domain 3 (CC3) in STIM1 activation. *Proc Natl Acad Sci USA* 112:6206–6211.
23. Wang X, et al. (2014) Distinct Orai-coupling domains in STIM1 and STIM2 define the Orai-activating site. *Nat Commun* 5:3183.
24. Zhou Y, et al. (2016) The STIM1-binding site nexus remotely controls Orai1 channel gating. *Nat Commun* 7:13725.
25. Hoover PJ, Lewis RS (2011) Stoichiometric requirements for trapping and gating of Ca^{2+} release-activated Ca^{2+} (CRAC) channels by stromal interaction molecule 1 (STIM1). *Proc Natl Acad Sci USA* 108:13299–13304.
26. Li Z, et al. (2011) Graded activation of CRAC channel by binding of different numbers of STIM1 to Orai1 subunits. *Cell Res* 21:305–315.
27. Miederer AM, et al. (2015) A STIM2 splice variant negatively regulates store-operated calcium entry. *Nat Commun* 6:6899.
28. Rana A, et al. (2015) Alternative splicing converts STIM2 from an activator to an inhibitor of store-operated calcium channels. *J Cell Biol* 209:653–669.
29. Hou X, Pedi L, Diver MM, Long SB (2012) Crystal structure of the calcium release-activated calcium channel Orai. *Science* 338:1308–1313.
30. Cai XY, et al. (2016) Orai1 concatemers reveal a hexameric Orai1 channel assembly. *Biophys J* 110:264a–265a.
31. Cai X, et al. (2016) The Orai1 store-operated calcium channel functions as a hexamer. *J Biol Chem* 291:25764–25775.
32. Yen M, Lokteva LA, Lewis RS (2016) Functional analysis of Orai1 concatemers supports a hexameric stoichiometry for the CRAC channel. *Biophys J* 111:1897–1907.
33. Wu MM, Covington ED, Lewis RS (2014) Single-molecule analysis of diffusion and trapping of STIM1 and Orai1 at endoplasmic reticulum-plasma membrane junctions. *Mol Biol Cell* 25:3672–3685.
34. Navarro-Borelly L, et al. (2008) STIM1-Orai1 interactions and Orai1 conformational changes revealed by live-cell FRET microscopy. *J Physiol* 586:5383–5401.
35. Wang Y, et al. (2009) STIM protein coupling in the activation of Orai channels. *Proc Natl Acad Sci USA* 106:7391–7396.
36. Perni S, Dynes JL, Yeromin AV, Cahalan MD, Franzini-Armstrong C (2015) Nanoscale patterning of STIM1 and Orai1 during store-operated Ca^{2+} entry. *Proc Natl Acad Sci USA* 112:E5533–E5542.
37. Brandman O, Meyer T (2008) Feedback loops shape cellular signals in space and time. *Science* 322:390–395.
38. Zhou Y, et al. (2009) The short N-terminal domains of STIM1 and STIM2 control the activation kinetics of Orai1 channels. *J Biol Chem* 284:19164–19168.
39. Ma HT, Venkatachalam K, Parys JB, Gill DL (2002) Modification of store-operated channel coupling and inositol trisphosphate receptor function by 2-amino-ethoxydiphenyl borate in DT40 lymphocytes. *J Biol Chem* 277:6915–6922.
40. Nwokonko RM, et al. (2017) Conformational coupling between STIM and Orai in the activation of store-operated Ca^{2+} entry. *Adv Exp Med Biol* 993:83–98.
41. Kar P, Parekh AB (2015) Distinct spatial Ca^{2+} signatures selectively activate different NFAT transcription factor isoforms. *Mol Cell* 58:232–243.
42. Dolmetsch RE, Lewis RS, Goodnow CC, Healy JI (1997) Differential activation of transcription factors induced by Ca^{2+} response amplitude and duration. *Nature* 386:855–858.
43. Dolmetsch RE, Xu K, Lewis RS (1998) Calcium oscillations increase the efficiency and specificity of gene expression. *Nature* 392:933–936.
44. Kar P, Bakowski D, Di Capite J, Nelson C, Parekh AB (2012) Different agonists recruit different stromal interaction molecule proteins to support cytoplasmic Ca^{2+} oscillations and gene expression. *Proc Natl Acad Sci USA* 109:6969–6974.
45. Kar P, et al. (2014) Dynamic assembly of a membrane signaling complex enables selective activation of NFAT by Orai1. *Curr Biol* 24:1361–1368.
46. Brandman O, Liou J, Park WS, Meyer T (2007) STIM2 is a feedback regulator that stabilizes basal cytosolic and endoplasmic reticulum Ca^{2+} levels. *Cell* 131:1327–1339.
47. Luik RM, Wang B, Prakriya M, Wu MM, Lewis RS (2008) Oligomerization of STIM1 couples ER calcium depletion to CRAC channel activation. *Nature* 454:538–542.
48. Ong HL, et al. (2015) STIM2 enhances receptor-stimulated Ca^{2+} signaling by promoting recruitment of STIM1 to the endoplasmic reticulum-plasma membrane junctions. *Sci Signal* 8:ra3.
49. Berna-Erro A, et al. (2009) STIM2 regulates capacitive Ca^{2+} entry in neurons and plays a key role in hypoxic neuronal cell death. *Sci Signal* 2:ra67.

BIOCHEMISTRY